Building and Environment 170 (2020) 106638

Contents lists available at ScienceDirect

Building and Environment

journal homepage: http://www.elsevier.com/locate/buildenv

Development and validation of a Monte Carlo-based numerical model for solar analyses in urban canyon configurations

Mattia Manni [a], Emanuele Bonamente [a,b], Gabriele Lobaccaro [c,*], Francesco Goia [c], Andrea Nicolini [a,b], Emmanuel Bozonnet [d,e], Federico Rossi [a,b]

[a] CIRIAF – Interuniversity Research Center on Pollution and Environment "Mauro Felli", Perugia, Italy
[b] Department of Engineering, University of Perugia, Perugia, Italy
[c] Department of Architecture and Technology, Faculty of Architecture and Design, Norwegian University of Science and Technology NTNU, Trondheim, Norway
[d] LaSIE (UMR CNRS 7356), University of La Rochelle, La Rochelle, France
[e] IRSTV (FR CNRS 2488), Nantes, France

ARTICLE INFO

Keywords:
Solar analyses
Full ray-tracing assessment
Monte Carlo method
2D urban canyon
Cool materials

ABSTRACT

Highly- and retro-reflective materials have recently been investigated and proposed as a new urban coating solution to reduce the so-called urban heat island effect. The present study aims at providing a numerical model for assessing inter-buildings solar reflections when these materials are applied to urban canyon's surfaces. The proposed model includes a function that accounts for sunray angle dependency of the solar reflectance, which is specifically important with regard to retro-reflective behavior. The novelty of this numerical model based on a Monte Carlo simulation approach implemented in the *Matlab* simulation environment is to conduct full ray-tracing solar analyses which can reproduce the energy exchange phenomena and simulate optical material properties. Experimental validation and inter-software comparison are carried out with measured data collected in an experimental facility in La Rochelle, France, in addition to simulation results from the *Radiance*-based *Diva for Rhino* tool. The results of the numerical model developed are in line with the values measured in the physical model (daily percent variation of 1.3% in summer) and within the boundary conditions defined in the present work. The residues, which were calculated for the hourly values throughout the day, are found to be in the range of ± 10 W/m^2, with the arithmetic average and standard deviation equal to – 2 W/m^2 and 7 W/m^2 respectively.

1. Introduction

Rising urban densification and global warming actively contribute to raising urban temperatures and increasing building energy demand for cooling [1–3]. The most recent census has found that around 54% of the world's population is currently living in cities, a number expected to reach 66% by 2050 [4]. Densified and altered urban patterns along with increased solar reflectance of building surfaces have the consequence of worsening the effect of inter-buildings solar reflections. This phenomenon, which concentrates a high amount of solar irradiance within the street environment [5–8] can lead to several issues amongst which the most documented one being the so-called Urban Heat Island (UHI) effect [9,10]. The main drivers of the UHI effect are anthropogenic heat, properties of the surface of the materials used in the built environment, the lack of permeable and vegetated surfaces in cities, and (higher) pollutant concentrations in the atmosphere [3,11–13]. Akbari et al. [6] reviewed the mitigation strategies proposed during the last three decades for tackling the over warming of the urban districts and defined cool materials and green infrastructures as the most promising technologies. The former aims at lowering the absorbed fraction of solar irradiance within the urban environment and the latter improves the evapotranspiration process and shading phenomena.

Following this, surface treatments characterized by high solar reflectance (ρ) have been investigated as potential cool materials. In particular, the influence of highly-reflective (HR) materials on urban microclimates has been assessed through numerical and physical models by demonstrating the related advantages (i.e. materials with low absorption coefficients) and disadvantages (i.e. an increased number of inter-buildings solar reflections) [14–16]. Recently, retro-reflective (RR) materials have been introduced as a sub-group of HR coatings which possess the ability to reflect back towards the sky dome most of the incident sun rays [17–22]. And although such a RR behavior permits overcoming some of the limitations observed in HR materials

* Corresponding author.
E-mail address: gabriele.lobaccaro@ntnu.no (G. Lobaccaro).

https://doi.org/10.1016/j.buildenv.2019.106638
Received 6 November 2019; Received in revised form 22 December 2019; Accepted 27 December 2019
Available online 29 December 2019

Nomenclature and acronyms table

UHI	urban heat island
HR	highly-reflective
RR	retro-reflective
UCM	urban canyon model
UDF	user-defined function
UC	urban canyon
ab	ambient bounces
NMBE	normalized mean bias error
CV(RMSE)	coefficient of variation of the root mean square error
R^2	coefficient of determination
H/W	height-to-width ratio
ρ	solar reflectance of the material
$Irr_{dir,hor}$	direct irradiation on horizontal surface
$Irr_{dif,hor}$	diffuse irradiation on horizontal surface
Irr_{out}	solar irradiation reflected out of the UC
c_v	coefficient of variation
σ	standard deviation
μ	arithmetic average
$\Delta_{\%}$	percent of variation
$Irr_{glob,hor}$	global solar irradiation on a horizontal surface
Irr_{pyr}	fraction of the Irr_{out}which can be measured by the pyranometer
W	width of the street
H	height of the buildings
k_t	clearness index
α_{sun}	solar altitude
T_{air}	outdoor air temperature
Φ	relative humidity
FE	finite element
$Irr_{glob,inc}$	global solar irradiation incident on a generic surface
Irr_{abs}	fraction of the $Irr_{glob,inc}$ which is absorbed by the surface
Irr_{trans}	fraction of the $Irr_{glob,inc}$ which is transmitted through the surface
Irr_{refl}	fraction of the $Irr_{glob,inc}$ which is reflected by the surface
α	absorption coefficient
ρ_d	reflection coefficient for the Lambertian diffusively reflected component
ρ_s	reflection coefficient for specular reflected component
ρ_{rr}	reflection coefficient for the retro-reflected component
θ	angle of incidence of the sunrays
$Irr_{out,dif}$	diffuse solar irradiation reflected out of the UC
Dif/Glob	diffuse solar irradiation to global solar irradiation ratio

applications, it still has the pitfall of reducing useful solar gains during the winter season [23,24]. For this reason, implementing a selective behavior on RR materials can represent a fundamental step in transitioning from traditional surface treatments to cool technologies [25]. Some concepts of selective RR materials have recently been proposed [26] along with methodologies to define their angular range of activation [25]. However, their impact on urban microclimates and mutual solar reflections between buildings has only been investigated in preliminary studies [27].

The main barrier to achieving a deeper understanding of the potential of RR materials is the lack of adequate tools to accurately model their optical properties. As reported in Table 1, existing software and urban canyon models (UCMs) present some limitations both in describing the complete energy exchange phenomena (i.e. *Diva for Rhino* can only assess short-wave solar irradiation) and in the assumptions used to simulate the material's optical properties (i.e. UCMs considers every material as optically diffuse). The different software used for solar analyses (e.g. *Diva for Rhino*, *Ladybug*, *Honeybee*, *Dragonfly*, *Radiance*, and *Daysim*) need to be coupled with other simulation engines to obtain a complete evaluation of the UC energy balance. Most of the time, this results in generating a virtual clone of the RR materials through a user-defined function (UDF) which must be specifically implemented for each surface treatment. When it comes to the UCMs, although the ones described in literature [28–31] assess various physical phenomena (in addition to short-wave energy exchanges), simplifications are still observed in the inter-buildings reflections assessment. In some studies, the surfaces are considered as isotropic reflectors [28,30], while in others they are considered as Lambertian diffuse surfaces [29,31]. Finally, in his most developed study of UCMs, Martilli [28] conducts solar analyses with a multi-layer urban canopy model intersecting atmospheric layers but the study still considers direct radiation only.

This research study aims at filling these knowledge gaps through the development and validation of a full ray-tracing numerical model for simulating inter-buildings short-wave solar reflections in an urban

Table 1
Summary of software tools and numerical models, including the model developed in this research, in which the simulated heat-transfer phenomena and materials are highlighted.

Tool's name	software/ numerical model	Simulated heat-transfer phenomena				Evapotranspiration	Simulated optical material properties		
		short-wave irradiation	long-wave irradiation	convection	conduction		Specularity	Diffusivity	Retro-reflection
Diva for Rhino	software	✓	–	–	–	–	✓	✓	–
Ladybug	software	✓	–	–	–	–	✓	✓	–
Honeybee	software	✓	✓	–	✓	–	✓	✓	–
Dragonfly	software	✓	✓	–	✓	–	✓	✓	–
Radiance	software	✓	–	–	–	–	✓	✓	–
Daysim	software	✓[a]	–	–	–	–	✓	✓	–
[28]	numerical model	✓	✓	✓	✓	✓	–	✓	–
[29]	numerical model	✓	✓	✓	✓	✓	–	✓	–
[30]	numerical model	✓	✓	✓	✓	✓	–	✓	–
[31]	numerical model	✓	✓	✓	✓	✓	–	✓	–
Proposed model	numerical model	✓	potential future development	potential future development	potential future development	potential future development	✓	✓	✓

[a] *Daysim* assesses the short-wave irradiation only in the indoor environment.

canyon (UC). Furthermore, the Monte Carlo-based routine implemented to model short-wave solar radiation can be applied (with some modifications) to the assessment of long-wave solar radiation as well, although this application has not been evaluated in this study. The numerical model proposed has a high degree of accessibility and allows users to directly interact and modify all the parameters defining the physical criteria which reflection events are based on (i.e. ray exit angles, light scattering pattern, material optical properties). The option to fully customize material properties is fundamental to enabling some of the key features in the model, such as introducing inter-dependency relationships for some of the parameters (i.e. angle of incidence of solar irradiation and reflection coefficient) or providing the possibility to modify the scattering phenomena. High flexibility and easy room for development are at the basis of the proposed algorithm: the assessment of short-wave solar irradiation can be integrated with the evaluation of long-wave irradiation analyses, the modelling of the energy fluxes through the façades, and the assessment of convective energy exchanges (Table 1). These features, in addition to the potential of modeling retro-reflective materials in accordance to the characterization protocols presented in the Literature [32–35], are the main strengths of using the proposed numerical model instead of using existing tools.

The numerical model also accounts for the impact of RR coatings – both traditional and selective – and of other cool materials (i.e. Lambertian diffuse HR, specular HR) on the solar irradiance reflected beyond the UC's boundary (Irr_{out}). In order to assess the reliability of the developed simulation approach, experimental data collected during a monitoring campaign [36] conducted in La Rochelle (France) are compared with the values estimated by the proposed numerical model to demonstrate its reliability. Furthermore, the limitations highlighted in the previous study [27] and referred to the evaluation of direct and diffuse solar irradiation contributions impinging on RR surfaces can be overcome by using the approach described here.

The main research domain covered by this work concerns:

i. The development of a numerical model that evaluates the effectiveness of the angular-selective RR materials described in Ref. [25].
ii. The validation of the Monte Carlo-based numerical model to simulate solar short-wave reflections events.
iii. The parameter setting of the model's simulation variables and the assessment of the outputs' uncertainty.

The paper is structured as follows: an introductory section that describes the numerical model (section 2) and which also explains more in detail the focus of the approach and input data (sub-section 2.1), the full ray-tracing solar assessment (sub-section 2.2), and the parameters setting for simulation (sub-section 2.3); a Methods section (section 3) articulated around four sub-sections and defining the workflow for the simulation and validation (sub-section 3.1), the experimental data (sub-section 3.2), the inter-software comparison (sub-section 3.3), and the validation indices (sub-section 3.4); a Result and Discussion section (section 4), where the experimental validation (sub-section 4.1) and the inter-software comparison (sub-section 4.2) are presented and discussed; and finally a Conclusions and future developments section which recapitulates the results and the implications of this work (section 5).

2. Monte Carlo-based numerical model

2.1. Approach and input data

The novelty of the developed numerical model is the application of a Monte Carlo method to full ray-tracing solar analyses in an urban context. Monte Carlo methods are more commonly applied to studies which require statistical analysis of data (simulation and validation) and are used to estimate probabilities associated with different scenarios [37–41]. In this work, Monte Carlo methods were used to estimate the solar irradiation collected by each element of an urban canyon as the probability that sun rays impinge on a surface – and are consequently absorbed or reflected – according to the input data.

The numerical model solves the energy conservation equation (Eq. (1)) by considering that the solar irradiation ($Irr_{glob,inc}$) on a surface equals the arithmetic sum of the absorbed (Irr_{abs}), the transmitted (Irr_{trans}) and the reflected fractions (Irr_{refl}). In the present research study, all the surfaces were considered as opaque so that the Irr_{trans} was equal to null. Furthermore, the Monte Carlo method contributed to solving the auxiliary equations (Eq. (2) and Eq. (3)) by quantifying the three Irr_{refl} contributions (i.e. Lambertian diffuse reflection, specular reflection, and retro-reflection).

$$Irr_{glob,inc} = Irr_{abs} + Irr_{refl} = Irr_{glob,inc}\cdot\alpha + Irr_{glob,inc}\cdot\rho = Irr_{inc}\cdot(\alpha+\rho) \quad \text{Eq. 1}$$

$$Irr_{refl} = Irr_{glob,inc}\cdot\rho = Irr_{glob,inc}\cdot(\rho_d + \rho_s + \rho_{rr}) \quad \text{Eq. 2}$$

$$\begin{aligned} Irr_{glob,inc} &= Irr_{glob,inc}\cdot(\alpha+\rho) \\ &= Irr_{glob,inc}\cdot(\alpha+\rho_d+\rho_s+\rho_{rr}) \rightarrow (\alpha+\rho_d+\rho_s+\rho_{rr}) = 1 \end{aligned} \quad \text{Eq. 3}$$

In terms of the geometrical configuration, a single-layer canopy model was implemented. The investigated scenario consisted of a two-dimensional, symmetrical street canyon with infinite length and customizable dimensions (building's height (H) and street's width (W)). The radiation assessment was a three-dimensional one as it also considered the variation of the sun azimuth throughout the day in addition to the canyon's orientation. The proposed model aims at simulating solar reflections within the street environment by reliably reproducing the optical properties of the coatings. It allows estimating the effectiveness of different UHI mitigation strategies in various scenarios during remarkable moments of the year (i.e. hour/day of the year characterized by the highest incident irradiation amount). Hence, the model is particularly useful in preliminary design stages when several alternative configurations, which are not yet completely defined, are compared to select the best one. Implementing additional equations also permits including in the calculation other energy exchange events or physical phenomena.

The input data required to run the solar assessments is reported in Table 2. This data is needed to input information about the urban canyon features and the atmospheric boundary conditions into the numerical model and allow setting the simulation variables.

When data about $Irr_{dir,hor}$ and $Irr_{dif,hor}$ was not available, the Reindl model [42,43] was exploited to calculate the diffuse to global irradiation ratio (Dif/Glob). This model uses a stepwise regression to select four significant predictors – clearness index (k_t), solar altitude (α_{sun}), outdoor air temperature (T_{air}), and relative humidity (Φ) – from a cluster of 28 potential predictor variables. Depending on the clearness index, three different equations (Eq. (4)-Eq. (6)) define the Dif/Glob ratio.

$$\begin{aligned} &0 \le k_t \le 0.30 \text{Dif/Glob} \\ &= 1.0 - 0.232\cdot k_t + 0.239\cdot\sin\alpha_{sun} - 0.000682\cdot T_{air} + 0.019\cdot\phi \end{aligned} \quad \text{Eq. 4}$$

$$\begin{aligned} &0.30 < k_t \le 0.78 \text{Dif/Glob} \\ &= 1.329 - 1.716\cdot k_t + 0.267\cdot\sin\alpha_{sun} - 0.00357\cdot T_{air} + 0.106\cdot\phi \end{aligned} \quad \text{Eq. 5}$$

$$k_t > 0.78 \text{Dif/Glob} = 0.426\cdot k_t + 0.256\cdot\sin\alpha_{sun} - 0.00349\cdot T_{air} + 0.0734\cdot\phi \quad \text{Eq. 6}$$

The $Irr_{dif,hor}$ was calculated by multiplying the measured $Irr_{glob,hor}$ by the Dif/Glob value (Eq. (7)) and subtracting this quantity from the $Irr_{glob,hor}$ (Eq. (8)).

$$Irr_{dif,hor} = \text{Dif/Glob}\cdot Irr_{glob,hor} \quad \text{Eq. 7}$$

$$Irr_{dir,hor} = Irr_{glob,hor} - Irr_{dif,hor} \quad \text{Eq. 8}$$

Table 2
Overview of the input parameters, which are grouped into three categories.

Input data	Symbol	Unit
Urban canyon features		
Height of the building	H	[m]
Width of the street	W	[m]
Height-to-width ratio of UC	H/W	unitless
Orientation of UC	O	[rad]
Surface absorption coefficient	α	[%]
Surface reflection coefficient for the Lambertian diffusively reflected component	ρ_d	[%]
Surface reflection coefficient for the specular reflected component	ρ_s	[%]
Surface reflection coefficient for the retro-reflected component	ρ_{rr}	[%]
Angular ranges to which the defined ρ-value is referred	$\Delta\theta$	[rad]
Boundary conditions		
Global solar irradiation on horizontal surface	$Irr_{glob,hor}$	[W m^{-2}]
Diffuse solar irradiation on horizontal surface	$Irr_{dif,hor}$	[W m^{-2}]
Direct solar irradiation on horizontal surface	$Irr_{dir,hor}$	[W m^{-2}]
Sun azimuth from the north	ϕ	[rad]
Sun elevation angle	θ	[rad]
Sun altitude	α_{sun}	[rad]
Clearness index	k_t	unitless
Outdoor air temperature	T_{air}	[K]
Relative humidity	Φ	[%]
Simulation variables		
Number of finite elements on a surface	FE	unitless
Number of simulated events	num_events	unitless
Ambient bounces number	ab	unitless

2.2. Full ray-tracing solar assessment

The procedure that allowed tracing sun rays starts by defining the FE through which the photon entered the UC and the corresponding entry angle. Each FE was univocally identified by a set of two values that referred to the surface it belonged to (street, buildings' façades, and UC ceiling) and its position on it (Fig. 1). Therefore, a random number between one and the total number of FEs on the UC top surface was generated to select the FE. In this process, the sun elevation angle was considered as the entry angle (when direct solar irradiance is assessed).

The next step of the procedure implemented in the numerical model was based on the previously described energy conservation equation (Eq. (1)). A random number between zero and one was generated to determine if the photon was "absorbed" or "reflected". The interval from zero to one was further divided into four sub-sections in which the boundaries described the probability of the photon being absorbed or reflected in different ways (Eq. (3)). These coefficients could be considered either as constants or as a function of other parameters (i.e. angle of incidence) and allowed simulating the behavior of RR materials and their solar reflectance.

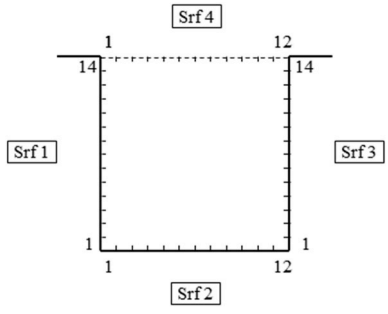

Fig. 1. Settings used for the spatial grid applied to the UC case study: the FEs on Srf 1 and Srf 3 varies from 1 to 14, while the FEs on Srf 2 and Srf 4 from 1 to 12.

The exit angle from the reflecting FE was estimated according to the reflection method computed in the Monte Carlo simulation (Fig. 2). The *Matlab* numerical model reiterated this part of the procedure until either the photon was absorbed, exited the canyon, or the maximum number of reflections (ab value) was reached. Thus, the algorithm was able to trace the path of each sun ray and calculate the number of events absorbed and reflected by each FE.

When it came to the full ray-tracing calculation of the diffuse solar irradiance, the initial entry angle – assigned to the photon entering the UC – was not correlated to the sun elevation as was the case for the direct solar irradiation, and was instead randomly generated. The same outputs, i.e. the number of absorbed and reflected photons for each FE, were computed for the diffuse irradiation analyses.

Finally, the number of absorbed and reflected photons was converted into quantities expressed in watt-hour per square meter (or watt per square meter when the estimated quantity refers to an hour) by considering $Irr_{dir,hor}$ and $Irr_{dif,hor}$. The output data characterized the incident solar irradiation per square meter of the one-meter-wide strip surface located in the middle of the UC, and this quantity was assumed to be representative of the irradiation along the entire canyon length.

It is worth mentioning that a function describing the accuracy of the pyranometer was also introduced into the procedure to validate the results of the numerical model against the experimental data. Therefore, the output parameter used for the validation stage was the Irr_{pyr} (a fraction of the Irr_{out}) instead of the Irr_{out}. When the photon hit the FE where the pyranometer was located (in the middle of the canyon ceiling), the entry angle was assessed. Then, the photon was measured (or not) by the device according to the instrument's response function.

2.3. Parameters setting for simulations

The influence of the pairs of values set for the simulation variables (ab setting and number of entering photons) on the output data from the *Matlab* numerical model (Irr_{out}) is investigated in this sub-section. At first, the number of photons (hereinafter referred to as "number of events") was kept constant – and equal to 10^5 – while the ab number was increased until all the events were fully-traced (absorbed before the cutoff). The resulting trends given by the number of fully-traced photons was assessed depending on the selected ab number and a percent of variation ($\Delta_{\%}$) from the plateau's value (amount of entering photons) was then assigned to each ab setting. Next, the ab number was considered equal to the greatest ab number investigated in the first step while the number of events was increased from 10^1 to 10^6 following a logarithmic scale. For each pair of values, the simulation was reiterated ten times to assess the c_v among the outcomes. The accuracy of the results was finally quantified according to the $\Delta_{\%}$ and the c_v.

The outcomes of the first part of this preliminary step looking at the parameter settings for simulations highlight that all the photons were absorbed by the canyon surfaces (façades, street, and ceiling) when the ab number was equal to 15. Furthermore, the number of events for which the tracing was not interrupted by the cutoff converges after six reflections to around 98,700 for both direct (Fig. 3a) and diffuse irradiation (Fig. 3b). When it comes to the estimated Irr_{out} (solar irradiation absorbed by urban canyon ceiling surface), the distribution of the results followed the same trend observed in the distribution of the events (Fig. 4): after six reflections, the resulting solar irradiation (201 W/m^2) tended to plateau towards the value calculated for 15 ambient bounces (207 W/m^2).

As a result, the ab number was chosen to be equal to six, which was the minimum value that guaranteed to maintain the $\Delta_{\%}$ from the function's plateau to less than 5.0%. This ab setting allowed reducing the computational time and provided a 3.0% underestimation within the assessment of the Irr_{out}.

As reported in Fig. 5, the results from the second part of the parameters setting stage were characterized by a c_v (calculated for the ten reiterations) that was inversely proportional to the number of events:

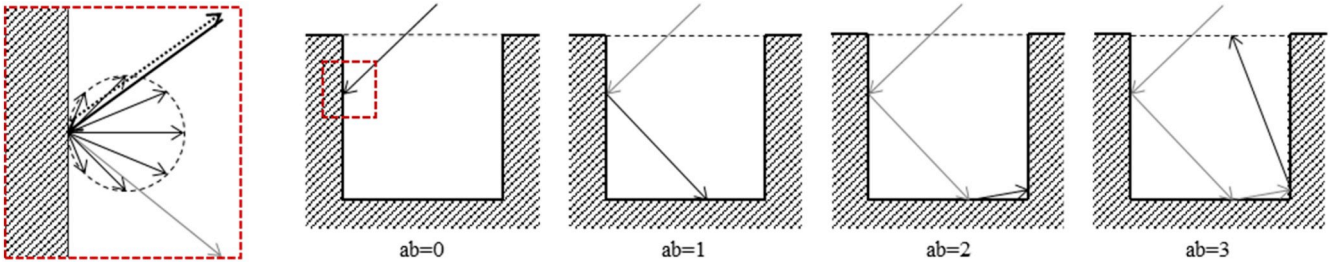

Fig. 2. On the left, overview of the different ways a surface interacts with incident photons (thick solid arrow). The photons can be reflected specularly (thin solid arrow), retro-reflected (dotted line), or diffusively reflected (all the arrows within the dashed circle). On the right, the visualization of the ray-tracing process depending on the considered ab values. In this example, the photon leaves the UC after three reflections.

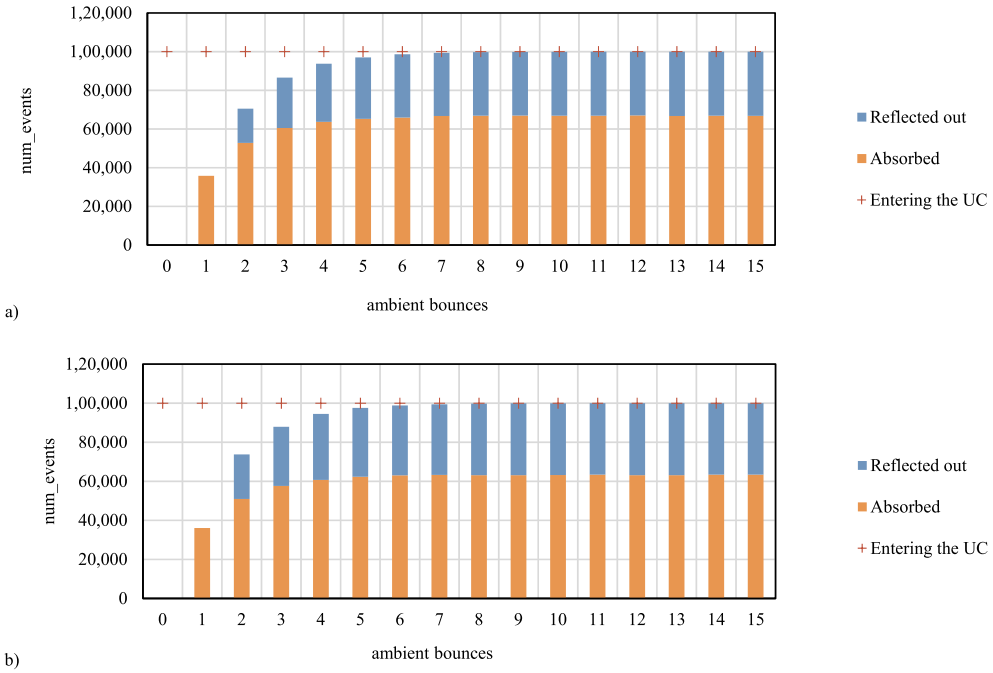

Fig. 3. Number of events absorbed by canyon surfaces and reflected out which are estimated by varying the ab value for the direct (a) and diffuse (b) solar irradiation.

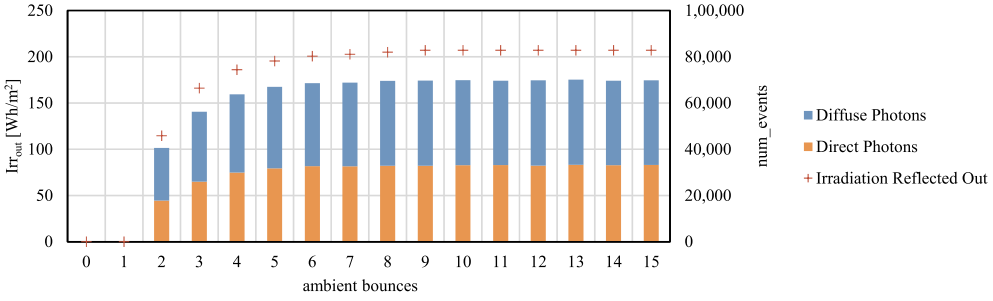

Fig. 4. Irr_{out} (global irradiation reflected out of the canyon) and the number of photons (for direct and diffuse irradiation) impinging on the top surface which are estimated by varying the ab value.

the highest value (155.5%) was observed for 10^1 photons entering the UC, while it was almost null (0.2%) in the case of 10^6 photons. The Irr_{out} quantities, which were estimated for the ten reiterations, varied from zero to 600 W/m^2 and from 207 W/m^2 to 208 W/m^2 when considering 10^1 and 10^6 events, respectively. Changing the number of events affected the computing time more than increasing the ab number: varying the ab number from six to 15 (with 10^6 events) caused the computing time to raise from 55.0 s to 60.0 s while reducing the number of events from 10^6 to 10^5 (with an ab number equal to 6) lowered it to 6.1 s. The reported time intervals referred to the solar analysis simulations, which were conducted for the time period of one hour. Thus, 10^5 events were selected to optimize the time necessary for running the simulation model without altering the results' accuracy ($c_v = 0.7\%$).

Finally, an additional sequence of ten reiterations was run by considering a previously identified pair of values: six ambient bounces and 10^5 events. The c_v was calculated to be 0.9% by considering the μ

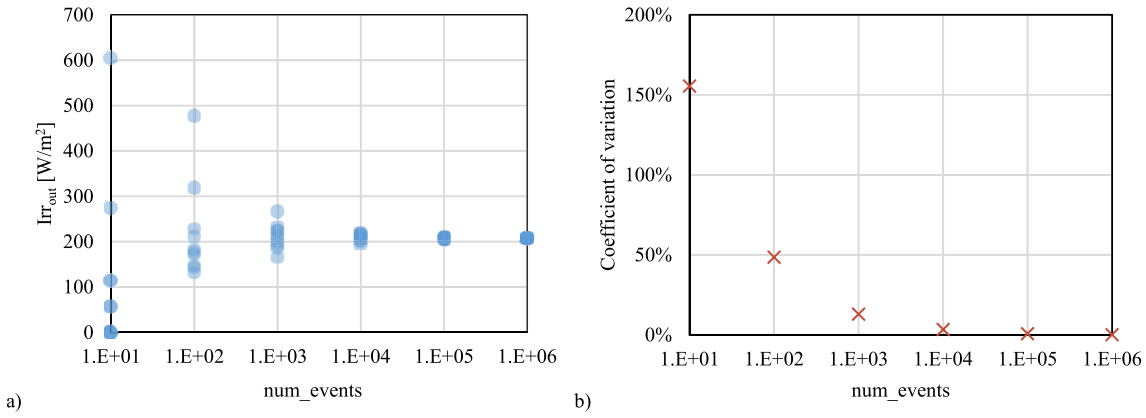

Fig. 5. Estimated Irr_{out} (a) and c_v among the results from the ten reiterations (b) which are calculated by varying the number of events.

and σ equal to 201 W/m^2 and 1.7 W/m^2, respectively. Hence, the relative error, which can be associated with the outcomes from *Matlab* numerical model, was estimated at 3.2% and calculated as the root sum square of the two aforementioned uncertainties (3.0% and 0.9%).

3. Methods for model validation

3.1. Workflow

The workflow followed in this research study was carried out in three steps, which focus on assessing the accuracy of the proposed numerical model developed in *Matlab* for the simulation of short-wave solar reflection events (Fig. 6).

In the initial step, the "parameters setting for simulations" was conducted for the proposed numerical model by focusing on the number of ambient bounces (amount of reflections considered by the tool in the ray-tracing analyses for each ray before the cutoff) and the number of photons entering the UC through the top surface. Several pairs of values (a pair consisting in one value for the ab number and one value for the number of events) were assessed to optimize the computational time while maintaining the results' uncertainty below a 5.0% threshold. The number of FE defined for the canyon ceiling was not investigated, while the other input data, which referred to the canyon features and boundary conditions, were set to match with the ones from the experimental facility. A Typical Meteorological Year or TMY weather data file obtained through the *EnergyPlus* weather (*.epw*)[1] of La Rochelle was used and the time of 11:00 a.m. on the 21st of August was selected during the preliminary research stage as the hour that best represented the most frequent environmental conditions observed during the monitoring campaign. The accuracy of the results was finally quantified according to the calculated $\Delta_{\%}$ and c_v.

The second step of the research method aimed at validating the *Matlab* numerical model against data collected during the monitoring campaign in La Rochelle. For the input parameters, the pyranometer features and the climate information collected by the weather station in situ were considered along with the input parameters from the preliminary step. At this stage of the research, the weather of the 21st of August (from 9 a.m. to 5 p.m.) was considered most representative of the climate conditions observed during that month under the monitoring campaign. The fraction of the hourly Irr_{out}, which was measured by the pyranometer (Irr_{pyr}), was assessed by the *Matlab* numerical model and results were validated against experimental data. The arithmetic differences (hereinafter referred to as "residues") and the $\Delta_{\%}$ between the two groups of Irr_{out} amounts (from *Matlab* numerical model and from the pyranometer) were estimated in order to define the mean value (μ), the standard deviation (σ), and other validation indices such as the Normalized Mean Bias Error (NMBE), the Coefficient of Variation of the Root Mean Square Error (CV(RMSE)), and the coefficient of determination (R^2).

In the third step, the outcomes from the *Matlab* numerical model were compared to the ones from *Diva for Rhino*. The input data was the same as the one described for the first stage, with the difference that *Diva for Rhino* could directly access the climate information without using another tool to visualize and process it (*Elements* software), unlike the numerical model. The time interval was extended in order to consider a wider range of climate conditions: the 21st of January (from 9 a.m. to 4 p.m.) and the 21st of August (from 6 a.m. to 7 p.m.) were chosen. The specific hourly amount of Irr_{out} was estimated by the numerical model and *Diva for Rhino*: both its spatial distribution on the UC's median and the average value were investigated. Then, the residues were assessed along to the $\Delta_{\%}$ values in order to define the μ and the σ numbers (outputs).

3.2. Experimental data

The experimental facility in La Rochelle [14] consisted of a platform on which several concrete empty tanks were arranged in five rows to simulate a sequence of scale buildings forming up to four UCs. Each building block was 5.00 m long, 1.30 m high, and 1.12 m wide, with an H/W around 1.2. The building façades were oriented alternately eastwards and westwards, and their surface treatments (white painting) was characterized by a 0.64 solar reflectance. The street was not treated with any material coating and had the same reflectance as the concrete tiles on the terrace (ρ = 0.36). Because this study only used the reference UC, which was the configuration with white painting applied to the façades (Fig. 7), the custom *Radiance* materials' properties, as well as the section of the *Matlab* script which described the ρ components of each FE, were set to simulate the behavior of Lambertian diffuse materials with the previously described features (ρ was 0.64 on building façades and 0.36 on the street paving).

The physical model was equipped with several measurement devices which permitted monitoring microclimatic variations in temperature, relative humidity, both short-wave and long-wave solar irradiation, and to observe hydric and thermal behaviors of the vegetated components (not present in the reference scenario). The sensors considered in this study were the ones designed for investigating short-wave solar irradiance reflected out of the urban canyon, and a complete description of the experimental instrumentations' layout can be found in Ref. [14]. The

[1] energyplus.net/weather.

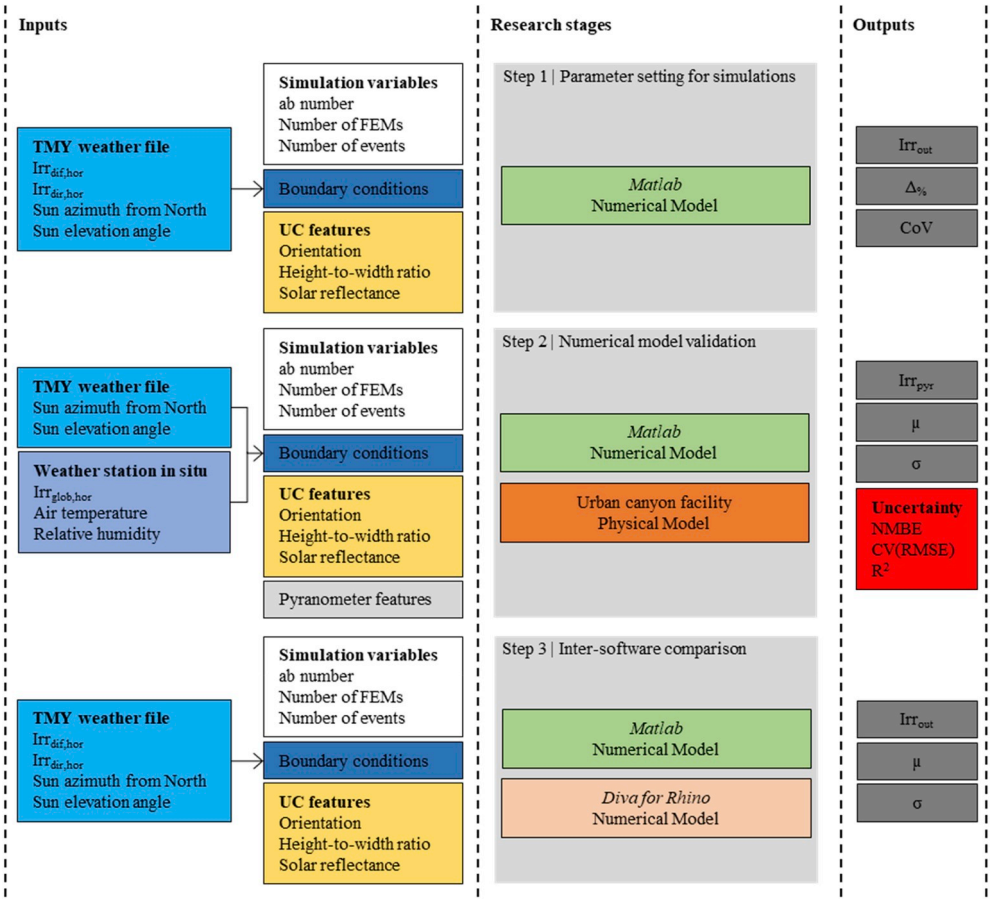

Fig. 6. Overview of the three steps followed in this study. The input data are classified as "simulation variables", "UC features", and "boundary conditions". The "boundary conditions" are grouped in turn depending on the source: "TMY weather file" and "weather station in situ".

Fig. 7. Experimental facility in La Rochelle: the five rows of empty tanks simulating four canyon environments and view of the sensors installed in the canyon median.

pyranometer[2]was placed above the street at the roof's height, in the middle of the canyon. A weather station was also installed in proximity to acquire meteorological quantities such as short-wave horizontal irradiation ($Irr_{glob,hor}$), outdoor air temperature, relative humidity, and cloud cover.

The CMP3 device is a Second Class pyranometer for short-wave solar irradiation measurement in the spectral range from 300 to 2800 nm. It is able to detect irradiance up to 2000 W/m^2 with a directional response (up to 80° with 1000 W/m^2 beam) lower than 20 W/m^2. According to the standard ISO 9060:2018, it is classified as "Spectrally Flat Class C". The measurement accuracy was estimated with a practical method[3] through the calculation of the root sum square of the critical performance criteria of the device. The Second Class pyranometer exploited in this study was characterized by a calibration uncertainty of 3.0% with a worst-case directional response error of 2.0% and a temperature response of 8.0%, coupled with an annual specific non-stability of 3.0%. Thus, the total uncertainty was quantified equal to 9.0% and was taken accounted for during the validation stage of the *Matlab* numerical model (sub-section 4.1).

3.3. Inter-software comparison

The inter-software comparison was conducted between the *Matlab* numerical model and the *Diva for Rhino* tool. The hourly amounts of solar irradiation incident on the UC top surface were evaluated by the *Diva for Rhino* software and compared with the quantities from the numerical model. The input data referring to the urban canyon features and the boundary conditions were defined according to the experimental facility in La Rochelle and kept constant throughout the study.

The grid of test points generated by *Diva for Rhino* to conduct solar

[2] Kipp & Zonen CMP3.
[3] ases.conference-services.net/.

analyses on the investigated surface was set at 0.1 m distance from the canyon ceiling (facing downward) with a cell size equal to 1 m by 1 m. The number of FEs on the top surface – equivalent to *Diva for Rhino*'s number of test points in the *Matlab* numerical model – was considered equal to 12 to guarantee an adequate discretization of the results and the correspondence with the grid of test points set for the geometry in *Diva for Rhino*.

When it comes to the other simulation variables, a complete overview of the 'rtrace' parameters employed in *Diva for Rhino* is shown in Table 3.

The ab number was set equal to five to estimate global irradiance composed by diffuse, direct and up to fifth-reflection contributions. This ab-setting guaranteed a good compromise between computational time and result accuracy since the estimated quantities steadily converged towards the most accurate value (which was found after seven ambient bounces with an increment lower than one percent) [44]. However, in the *Matlab* numerical model, the ab number was set equal to 6, while 10^5 events were considered to simulate the photons of the direct and diffuse irradiation ($2{\cdot}10^5$ events total). These values were defined following the analysis conducted during the parameters setting for simulations stage (sub-section 2.3).

3.4. Validation indices

The degree of confidence for the numerical model was measured through some validation indices following the ASHRAE Guideline 14 [45] such as the NMBE, the CV(RMSE), and the R^2 parameters.

The NMBE number – expressed as a percentage – provides an understanding of whether a generic amount of n simulated values (s_i) over- or under-predict the measured ones (m_i), and is calculated as:

$$NMBE = \frac{1}{\overline{m}} \cdot \frac{\sum_{i=1}^{n}(m_i - s_i)}{n-1} \cdot 100$$

The CV(RMSE) percentage parameter measures the variability of the error between measured and simulated data and is generally coupled to the NMBE to verify the accuracy of the models. It is calculated as:

$$CV(RMSE) = \frac{1}{\overline{m}} \cdot \sqrt{\frac{\sum_{i=1}^{n}(m_i - s_i)^2}{n-1}} \cdot 100$$

The third statistical value is the R^2 which is a number between zero and one and indicates how close simulated values are to the regression line of the measured values. It is calculated as:

$$R^2 = \left(\frac{n \cdot \sum_{i=1}^{n} m_i \cdot s_i - \sum_{i=1}^{n} m_i \cdot \sum_{i=1}^{n} s_i}{\sqrt{\left(n \cdot \sum_{i=1}^{n} m_i^2 - \sum_{i=1}^{n} (m_i)^2\right) \cdot \left(n \cdot \sum_{i=1}^{n} s_i^2 - \sum_{i=1}^{n} (s_i)^2\right)}} \right)^2$$

When it comes to the calibration criteria for the hourly time interval, according to the ASHRAE Guideline 14 [45], a high degree of confidence can be assigned to the numerical model if:

i. the NMBE number is included within the range from −10% to 10%;
ii. the CV(RMSE) is lower than 30%;
iii. the R^2 is higher than 0.75.

Table 3
Set of 'rtrace' parameters employed for conducting solar radiation analyses with Diva for Rhino.

Ambient bounces	Ambient divisions	Ambient super samples	Ambient resolution	Ambient accuracy
5	1000	20	300	0.1

4. Results and discussion

4.1. Experimental validation

The proposed numerical model was validated by comparing the Irr_{pyr} amounts estimated by the numerical model to the quantities measured in La Rochelle's experimental facility.

The hourly outputs elaborated by the downward-facing pyranometer refer to the short-wave irradiation leaving the canyon in the middle of its median, and they are reported in Table 4 along with the global irradiation impinging on a horizontal surface (monitored by the weather station in situ). The hourly distribution of the collected data throughout the day showed a peak at 3.00 p.m. (200 W/m^2) when the weather station measured around 770 W/m^2 of solar global irradiation incident on a horizontal surface. As discussed in subsection 3.2, the pyranometer's measurements were affected by a 9.0% uncertainty, which caused an absolute error ranging from ±9 W/m^2 (at 9.00 a.m.) to ±18 W/m^2 (at 3.00 p.m.).

Regarding the numerical model, the hourly results from the solar analyses – conducted considering the same conditions of the experimental facility – are reported in Table 4. The daily peak of the Irr_{pyr} was found at 3.00 p.m. (the same as in the distribution of the pyranometer's measurements) and equal to 205 W/m^2. The two distributions of the hourly amounts of Irr_{pyr} (*Matlab* numerical model and pyranometer's measurements) showed the same trend: they are shown overlapping each other in Fig. 8a by considering the respective uncertainties (around 3.0% for the numerical model and 9.0% for output data from the pyranometer). The graph highlights how the simulated Irr_{pyr} amounts – and the respective error bars based on the algorithm's uncertainty – were well within the interval defined by the measured solar irradiation and the respective absolute error. For instance, the Irr_{pyr} assessed by the numerical model at 11.00 a.m. was equal to 170 ± 5 W/m^2 which is consistent with the interval 180 ± 7 W/m^2 determined during the monitoring campaign. The analyses of residues calculated from the nominal values highlighted how these values could vary between −10 W/m^2 and +10 W/m^2, with the μ and the σ equal to −2 W/m^2 and 7 W/m^2, respectively.

The uncertainty analysis conducted considering the measured and the simulated values reported in Table 4 highlighted that the NMBE and the CV(RMSE) numbers were equal to −1% and 4%, respectively; while the R^2 is 0.97. Hence, the developed numerical model is characterized by a high degree of confidence according to the limits presented in ASHRAE Guideline 14 and discussed in sub-section 3.4.

Finally, the $\Delta_{\%}$ between the Irr_{pyr} estimated by *Matlab* numerical model throughout the day of the 21st of August and the measured quantity from the experimental facility were investigated. The daily value of the $\Delta_{\%}$ was equal to about 1.3% and it was calculated considering the daily Irr_{pyr} quantified by the proposed numerical model and the pyranometer: 1500 ± 50 Wh/m^2 and 1520 ± 140 Wh/m^2, respectively.

4.2. Inter-software comparison

The reliability of the results (Irr_{out}) carried out by the numerical model is here discussed through a comparison with outcomes assessed by the *Radiance*-based software *Diva for Rhino*, for summer (21st of January) and winter (21st of July) conditions.

The solar analyses conducted for the 21st of January from 9.00 a.m. to 4.00 p.m. showed the minimum overall difference between the hourly outcomes from the two tools. The residues ranged from −5 W/m^2 (12.00 p.m. and 2.00 p.m.) to 5 W/m^2 (4.00 p.m.), with a null value at 9.00 a.m. (when both *Matlab* and *Diva for Rhino* numerical models quantify the Irr_{out} equal to 84 W/m^2) (Fig. 9b). The daily trends of the Irr_{out} are depicted in Fig. 9a: the numerical model estimated the peak (124 W/m^2) at 1.00 p.m., while *Diva for Rhino* software considered it to happen at 12.00 p.m. (125 W/m^2). Moreover, the $\Delta_{\%}$ among the two series of

Table 4
Global solar irradiation amounts that were measured by devices installed in the physical model (i.e. weather station, pyranometer) or estimated by the proposed algorithm.

	Source		9.00 a.m.	10.00 a.m.	11.00 a.m.	12.00 p.m.	1.00 p.m.	2.00 p.m.	3.00 p.m.	4.00 p.m.	5.00 p.m.
Global irradiation on horizontal surface	Weather station	W/m^2	313	486	630	684	774	802	772	679	580
Global irradiation reflected out of the UC	Pyranometer	W/m^2	95 ± 9	155 ± 14	180 ± 17	170 ± 16	170 ± 16	175 ± 16	200 ± 18	190 ± 17	180 ± 17
	Numerical model	W/m^2	90 ± 3	145 ± 5	170 ± 5	170 ± 5	165 ± 5	170 ± 5	205 ± 6	200 ± 6	180 ± 6

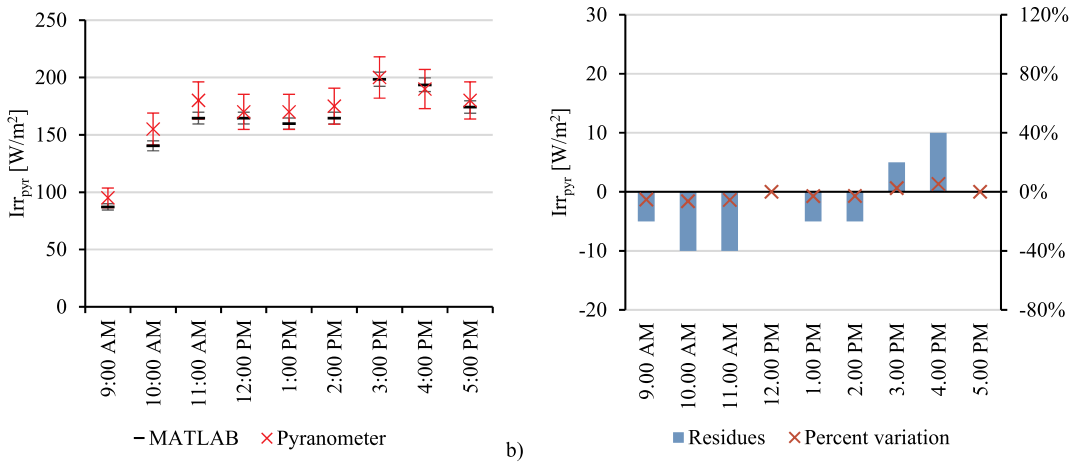

Fig. 8. On the left, hourly solar irradiation leaving the canyon with the respective absolute errors (a) which have been calculated by the *Matlab* model and measured by the pyranometer in summer conditions. On the right, distribution of residues and percent variations through the day (b).

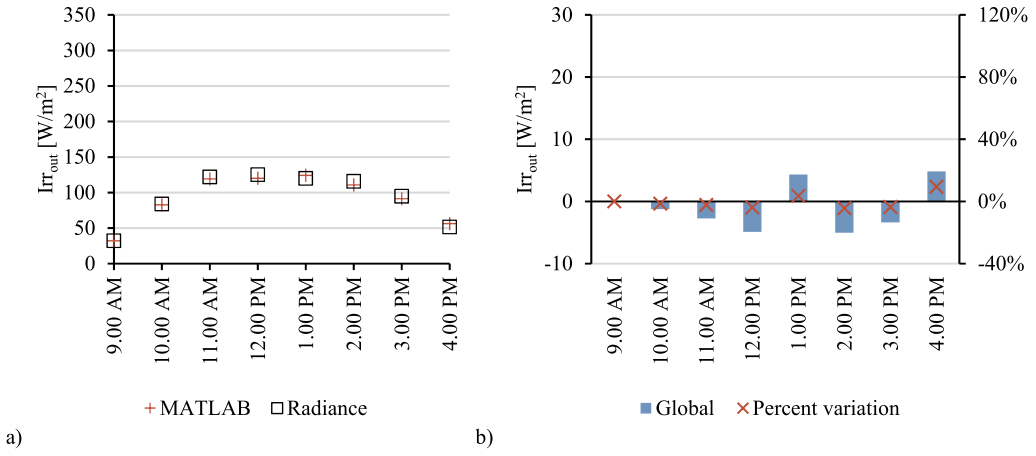

Fig. 9. Hourly Irr$_{out}$ (a) calculated by *Matlab* numerical model and *Diva for Rhino* software in winter conditions with the respective residues and $\Delta_{\%}$ quantities (b).

values ranged from −4.0% (12.00 p.m., 2.00 p.m., and 3.00 p.m.) to +9.0% (4.00 p.m.), while their μ was null and the respective σ equal to 5.0%.

Finally, the Irr$_{out}$ estimated throughout the day was 736 Wh/m^2 according to *Matlab* numerical model and 745 Wh/m^2 according to *Diva for Rhino*, with $\Delta_{\%}$ of around −1.0%.

On Fig. 10 the fraction of Irr$_{out}$ impinging on each FE (or test point, in *Diva for Rhino* environment) of the top surface are reported for the three hours (10.00 a.m., 1.00 p.m., and 4.00 p.m.) representing several different moments of the day (early morning, midday, and late afternoon). On this figure, it is possible to observe that the quantities estimated by the numerical model for the FEs which are close to the two façades (ID_FE values are 1, 2, 11, and 12) are the ones that diverged the most from *Diva for Rhino*'s values (residues achieve 65 W/m^2). However, the rest of the two distributions were similar (residues range from −18 W/m^2 to 6 W/m^2) and characterized by the same trend (monotone decay at 10.00 a.m., almost constant at 1.00 p.m., and monotone growth at 4.00 p.m.).

In the assessment of the Irr$_{out}$ on the 21st of August, the number of hours considered in the simulations was increased to match the longer time interval of available daylight. As mentioned in the previous paragraph, the difference between output data from the two tools was greater in summer than in winter conditions. The residues ranged from −4 W/m^2 (7.00 a.m.) to 23 W/m^2 (2.00 p.m.) and remained higher than

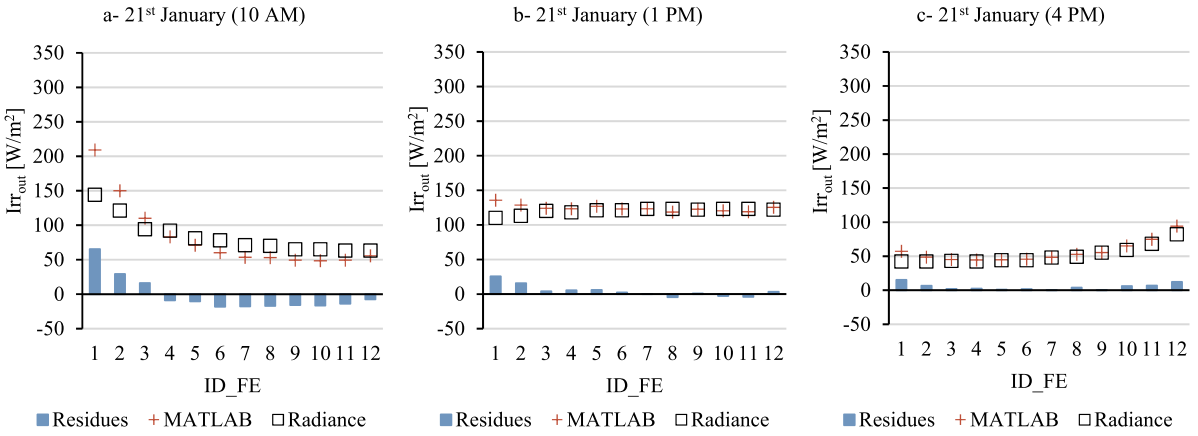

Fig. 10. Global solar irradiation impinging on FEs of the top surface at 10.00 a.m. (a), 1.00 p.m. (b), and 4.00 p.m. (c), and respective residues between results from the numerical model and *Diva for Rhino* software.

9 W/m^2 during most of the daytime (from 8.00 a.m. to 6.00 p.m.) (Fig. 11b). The $\Delta_{\%}$ was always lower than 10.0% between 8.00 a.m. and 6.00 p.m. (μ and σ equal to 8.0% and 4.0%, respectively) because of the higher amounts of solar irradiance involved in the calculation. Conversely, the lower available solar irradiance negatively influenced the $\Delta_{\%}$ quantities during the rest of the day which peaked (34.0%) at 6.00 a.m. If the whole day was considered, both the μ and the σ calculated for the $\Delta_{\%}$ values raised to 11.0%. The Irr_{out} values were maximal at 1.00 p.m. in both simulations (275 W/m^2 and 295 W/m^2, according to *Diva for Rhino* and *Matlab* numerical models, respectively) and slowly decreased towards null values at 6.00 a.m. (3 W/m^2 and 4 W/m^2) and 7.00 p.m. (17 W/m^2 and 22 W/m^2) (Fig. 11a). The outcomes carried out by the numerical model diverged the most from the references (highest residues) in two intervals: from 8.00 a.m. to 10.00 a.m. and from 1.00 p.m. to 2.00 p.m. (around 10.0% higher).

In the summer scenario, the solar irradiation leaving the UC during the day ranged from 2218 Wh/m^2 to 2380 Wh/m^2 depending on the simulation engine exploited for the calculation: *Radiance* in the first case and the Monte Carlo method in the second. The consequent $\Delta_{\%}$ (7.0%) turned out to be higher than in winter.

The hourly solar irradiation impinging on each FE was evaluated at 9.00 a.m., 1.00 p.m., and 5.00 p.m. on the 21st of August. As observed in the winter scenario, the main divergences were found in the proximity of the two façades (ID_FE are 1, 2, 11, and 12) where the absolute amounts of the residues ranged from 9 W/m^2 to 62 W/m^2. Conversely, the same trends (monotone decay at 9.00 a.m., almost constant at 1.00 p.m., and monotone growth at 5.00 p.m.) were seen for the remaining elements of the distributions (Fig. 12).

The comparison between results from the numerical model and the ones from *Diva for Rhino* permitted verifying the reliability of the proposed script both in summer and in winter conditions. The accuracy of the results and the appropriateness of the Monte Carlo method to simulate solar short-wave reflections events was confirmed at this stage by the low $\Delta_{\%}$ amounts and residues observed in the analyses of the hourly Irr_{out} as well as of the amounts of solar irradiation impinging on FEs during three representative hours of the day.

4.3. Considerations on the uncertainty of the Monte-Carlo based model

The double validation process (experimental validation and inter-software comparison) of outputs given by the *Matlab* numerical model is here summarized based on the parameters reported in Table 5.

The validation process against experimental data showed that the *Matlab* numerical model was quite accurate when summer boundary conditions were simulated, although it tended to slightly under-predict solar irradiation reflected in the UC (μ calculated for residues equals −2.0%) with a low dispersion of the results (σ calculated for residues is 4.0%). The degree of confidence demonstrated by the numerical model was also confirmed by the evaluated validation indices: the NMBE and the CV(RMSE) numbers, and the R^2 coefficient complied with the acceptability criteria from ASHRAE Guideline 14 (Table 6).

When it comes to the inter-software comparison, the solar analyses conducted by the numerical model and the ones from *Diva for Rhino* tool for summer season highlighted that the former over-estimates the solar

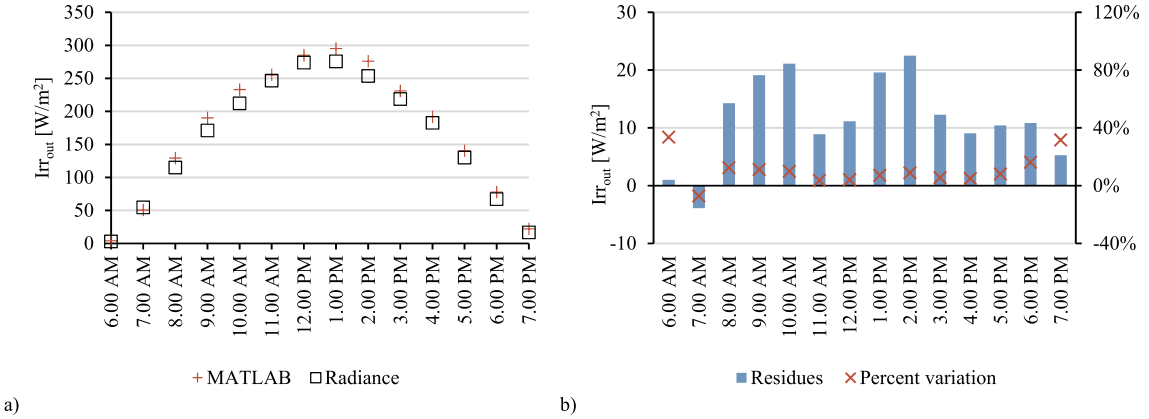

Fig. 11. Hourly Irr_{out} (a) calculated by *Matlab* numerical model and *Diva for Rhino* software in summer conditions with the respective residues and $\Delta_{\%}$ quantities (b).

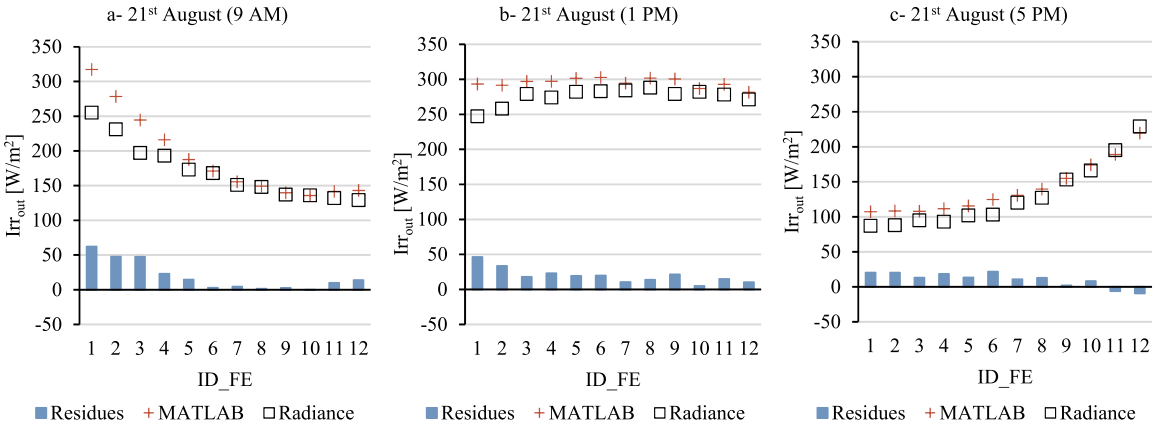

Fig. 12. Global solar irradiation impinging on FEs of the top surface at 10.00 a.m. (a), 1.00 p.m. (b), and 4.00 p.m. (c), and respective residues between results from the numerical model and *Diva for Rhino* software.

Table 5
Overview of the μ and σ numbers estimated for the residues during the validation research stages and the inter-software comparison.

Measure unit	Experimental validation		Inter-software comparison			
	Summer condition (21st August)		Winter condition (21st January)		Summer condition (21st August)	
	μ	σ	μ	σ	μ	σ
%	−2	4	–	5	8	4
W/m²	−2	7	−1	4	14	5

Table 6
Uncertainty parameters and acceptability criteria from ASHRAE Guideline 14.

Uncertainty parameters	Acceptability criteria (ASHRAE Guideline 14)		Estimated amount
	Lower limit	Upper limit	
NMBE	−10%	10%	−1%
CV(RMSE)	0%	30%	4%
R^2	0.75	1.00	0.97

irradiation (μ achieves 8.0%) with a negligible result's dispersion (σ is 4.0%). However, when winter conditions were considered, the simulation results from the two tools did not significantly differ (μ is null and σ equals 5.0%).

5. Conclusions and future developments

An innovative algorithm for conducting full ray-tracing solar analyses in the *Matlab* environment by implementing a Monte Carlo-based routine has been described and validated in the present research study. The numerical model represents an important step in the enhancement of tools for conducting full ray-tracing solar analyses as well as in the development of RR technologies and their application as urban coatings. Its main strength is that it allows assessing the influence of RR materials on the energy balance of UCs by accessing all the physical variables which regulate reflection events. The high accessibility of the material properties, the full ray-tracing assessment, and the possible introduction in the calculation of other physical phenomena describing energy exchanges make this model more advantageous than other existing tools which present some simplifications (i.e. considering all the surfaces as diffuse reflectors) or limitations (i.e. evaluating only short-wave irradiation).

Furthermore, the developed model includes a function that allows varying the coefficients of reflection (ρ_d, ρ_s, and ρ_{rr}) – defining both the typology (Lambertian diffuse, specular, retro-reflection) and the magnitude of the phenomenon – depending on the angle of incidence of the sun rays. This function permits to replicate the advanced engineered retro-reflective materials and to create a virtual clone whose properties are defined according to the several protocols found in the Literature [32–35]. This guarantees a virtual clone extremely close to reality.

The reliability of the Monte Carlo method to simulate short-wave reflections events was demonstrated through a double validation process during which simulation outcomes were compared to data measured in the physical urban canyon model in La Rochelle and processed through an inter-software comparison carried out using the *Diva for Rhino* tool.

The main findings were that:

- Setting the ambient bounces value equal to six and the number of events as 10^5 permitted reducing up to ten times the computational time required by the numerical model (from 60.0 s with ab 15 and 10^6 events to 6.1 s with ab six and 10^5 events) while maintaining the uncertainty below the 5.0% threshold.
- The Irr_{pyr} values estimated through the proposed numerical model were consistent with the quantities measured by pyranometer (daily $\Delta_{\%}$ equal to 1.3%);
- The hourly $\Delta_{\%}$ between the numerical model's outcomes and *Diva for Rhino*'s ones were characterized by a null μ-value and a σ of 5.0% in winter, and a μ-value of 8.0% and a σ = 4.0% in summer.

In conclusion, the Monte Carlo method has demonstrated to be as valid as others (*Diva for Rhino*) which are validated methods and largely applied in research studies of solar analyses. The numerical model was also proven to be coherent with the physical model in La Rochelle (France) within the boundary conditions defined in the present work.

As far as the future developments are concerned, the *Matlab* numerical model can be applied (i) to investigate optical issues (glare) related to the exploitation of high- and retro-reflective materials as surface treatment within the built environment, (ii) to evaluate the potentials of retro-reflective technologies in different climate contexts (with different solar geometries), and (iii) to assess the influences of parameters such as the aspect height-to-width ratio and the surface solar reflectance on the amount of solar irradiation reflected beyond the urban canyon when comparing several scenarios. Moreover, the *Matlab* numerical model can be further enhanced by (iv) including in the calculation other energy exchange phenomena such as long-wave radiation assessment, convective exchanges, and conduction heat transfer.

Acknowledgments

The authors wish to thank the Norwegian University of Science and Technology (Trondheim, Norway), the University of Perugia (Perugia, Italy) and the CIRIAF – Interuniversity Research Center on Pollution and Environment "Mauro Felli" for supporting the collaboration between the two universities in this work, framed in the EU program for education, training, youth and sport – 'ERASMUS+'. The authors also wish to thank the research group coordinated by professor Emmanuel Bozonnet for having agreed to share the data collected during the monitoring campaign in La Rochelle.

References

[1] M. Santamouris, C. Cartalis, A. Synnefa, D. Kolokotsa, On the impact of urban heat island and global warming on the power demand and electricity consumption of buildings - a review, Energy Build. 98 (2015) 119–124, https://doi.org/10.1016/j.enbuild.2014.09.052.
[2] D. Zhou, L. Zhang, D. Li, D. Huang, C. Zhu, Climate–vegetation control on the diurnal and seasonal variations of surface urban heat islands in China, Environ. Res. Lett. 11 (2016), https://doi.org/10.1088/1748-9326/11/7/074009.
[3] C. Piselli, V.L. Castaldo, I. Pigliautile, A.L. Pisello, F. Cotana, Outdoor comfort conditions in urban areas: on citizens' perspective about microclimate mitigation of urban transit areas, Sustain. Cities Soc. 39 (2018) 16–36, https://doi.org/10.1016/J.SCS.2018.02.004.
[4] D. of E. and S.A. United Nations, World Urbanization Prospects: the 2014 Revision, Highlights, 2014. https://esa.un.org/unpd/wup/.
[5] I. Lima, V. Scalco, R. Lamberts, Estimating the impact of urban densification on high-rise office building cooling loads in a hot and humid climate, Energy Build. 182 (2019) 30–44, https://doi.org/10.1016/J.ENBUILD.2018.10.019.
[6] H. Akbari, D. Kolokotsa, Three decades of urban heat islands and mitigation technologies research, Energy Build. 133 (2016) 834–842, https://doi.org/10.1016/J.ENBUILD.2016.09.067.
[7] K.I. Brans, J.M.T. Engelen, C. Souffreau, L. De Meester, Urban hot-tubs: local urbanization has profound effects on average and extreme temperatures in ponds, Landsc. Urban Plan. 176 (2018) 22–29, https://doi.org/10.1016/J.LANDURBPLAN.2018.03.013.
[8] L. Lin, E. Ge, X. Liu, W. Liao, M. Luo, Urbanization effects on heat waves in Fujian Province, Southeast China, Atmos. Res. 210 (2018) 123–132, https://doi.org/10.1016/J.ATMOSRES.2018.04.011.
[9] M.A. Rahman, A. Moser, T. Rötzer, S. Pauleit, Microclimatic differences and their influence on transpirational cooling of Tilia cordata in two contrasting street canyons in Munich, Germany, Agric. For. Meteorol. 232 (2017) 443–456, https://doi.org/10.1016/J.AGRFORMET.2016.10.006.
[10] X. Xu, J.E. González, S. Shen, S. Miao, J. Dou, Impacts of urbanization and air pollution on building energy demands — Beijing case study, Appl. Energy 225 (2018) 98–109, https://doi.org/10.1016/J.APENERGY.2018.04.120.
[11] C.M.J. Warren, Heat islands; understanding and mitigating heat in urban Areas20122Lisa Gartland. Heat islands, in: Understanding and Mitigating Heat in Urban Areas, Earthscan, London, 2011, p. 192, https://doi.org/10.1108/pm.2012.30.1.105.2, 978-1-84971-298-9 $64.95 Prop. Manag. 30 (2014) 105–106.
[12] T.R. Oke, Canyon geometry and the nocturnal urban heat island: comparison of scale model and field observations, J. Climatol. 1 (1981) 237–254, https://doi.org/10.1002/joc.3370010304.
[13] X. Xie, Z. Huang, J. Wang, Z. Xie, The impact of solar radiation and street layout on pollutant dispersion in street canyon, Build. Environ. 40 (2005) 201–212, https://doi.org/10.1016/j.buildenv.2004.07.013.
[14] M. Doya, E. Bozonnet, F. Allard, Experimental measurement of cool facades' performance in a dense urban environment, Energy Build. 55 (2012) 42–50, https://doi.org/10.1016/J.ENBUILD.2011.11.001.
[15] H. Taha, Urban climates and heat islands: albedo, evapotranspiration, and anthropogenic heat, Energy Build. 25 (1997) 99–103, https://doi.org/10.1016/S0378-7788(96)00999-1.
[16] H. Radhi, S. Sharples, E. Assem, ARTICLE IN PRESS G Model Impact of urban heat islands on the thermal comfort and cooling energy demand of artificial islands—A case study of AMWAJ Islands in Bahrain, https://doi.org/10.1016/j.scs.2015.07.017, 2015.
[17] J. Yuan, K. Emura, C. Farnham, Potential for Application of Retroreflective Materials Instead of Highly Reflective Materials for Urban Heat Island Mitigation, 2016, https://doi.org/10.1155/2016/3626294.
[18] H. Sakai, K. Emura, N. Igawa, Reduction of reflected heat by retroreflective materials, J. Struct. Constr. Eng. (Transactions AIJ) 73 (2008) 1239–1244, https://doi.org/10.3130/aijs.73.1239.
[19] F. Rossi, A.L. Pisello, A. Nicolini, M. Filipponi, M. Palombo, Analysis of retro-reflective surfaces for urban heat island mitigation: a new analytical model, Appl. Energy 114 (2014) 621–631, https://doi.org/10.1016/j.apenergy.2013.10.038.
[20] H. Akbari, A.G. Touchaei, Modeling and labeling heterogeneous directional reflective roofing materials, Sol. Energy Mater. Sol. Cells 124 (2014) 192–210, https://doi.org/10.1016/j.solmat.2014.01.036.
[21] F. Rossi, B. Castellani, A. Presciutti, E. Morini, M. Filipponi, A. Nicolini, M. Santamouris, Retroreflective Façades for Urban Heat Island Mitigation: Experimental Investigation and Energy Evaluations, 2015, https://doi.org/10.1016/j.apenergy.2015.01.129.
[22] E. Morini, B. Castellani, A. Nicolini, F. Rossi, U. Berardi, Effects of aging on retro-reflective materials for building applications, Energy Build. 179 (2018) 121–132, https://doi.org/10.1016/j.enbuild.2018.09.013.
[23] A. Vallati, L. Mauri, C. Colucci, Impact of shortwave multiple reflections in an urban street canyon on building thermal energy demands, Energy Build. 174 (2018) 77–84, https://doi.org/10.1016/J.ENBUILD.2018.06.037.
[24] L. Mauri, G. Battista, E. de Lieto Vollaro, R. de Lieto Vollaro, Retroreflective materials for building's façades: experimental characterization and numerical simulations, Sol. Energy 171 (2018) 150–156, https://doi.org/10.1016/j.solener.2018.06.073.
[25] M. Manni, G. Lobaccaro, F. Goia, A. Nicolini, An inverse approach to identify selective angular properties of retro-reflective materials for urban heat island mitigation, Sol. Energy 176 (2018) 194–210, https://doi.org/10.1016/J.SOLENER.2018.10.003.
[26] H. Sakai, H. Iyota, Development of Two New Types of Retroreflective Materials as Countermeasures to Urban Heat Islands, 2017, https://doi.org/10.1007/s10765-017-2266-y.
[27] M. Manni, G. Lobaccaro, F. Goia, A. Nicolini, F. Rossi, Exploiting selective angular properties of retro-reflective coatings to mitigate solar irradiation within the urban canyon, Sol. Energy 189 (2019) 74–85, https://doi.org/10.1016/J.SOLENER.2019.07.045.
[28] A. Martilli, A. Clappier, M.W. Rotach, An urban surface exchange parameterisation for mesoscale models, Boundary-Layer Meteorol. 104 (2002) 261–304, https://doi.org/10.1023/A:1016099921195.
[29] H. Kusaka, H. Kondo, Y. Kikegawa, F. Kimura, A simple single-layer urban canopy model for atmospheric models: comparison with multi-layer and slab models, Boundary-Layer Meteorol. 101 (2001) 329–358, https://doi.org/10.1023/A:1019207923078.
[30] V. Masson, A physically-based scheme for the urban energy budget in atmospheric models, Boundary-Layer Meteorol. 94 (2000) 357–397, https://doi.org/10.1023/A:1002463829265.
[31] Z.-H. Wang, E. Bou-Zeid, J.A. Smith, A coupled energy transport and hydrological model for urban canopies evaluated using a wireless sensor network, Q. J. R. Meteorol. Soc. 139 (2013) 1643–1657, https://doi.org/10.1002/qj.2032.
[32] J. Yuan, C. Farnham, K. Emura, Development of a retro-reflective material as building coating and evaluation on albedo of urban canyons and building heat loads, Energy Build. 103 (2015) 107–117, https://doi.org/10.1016/j.enbuild.2015.06.055.
[33] E. Morini, B. Castellani, A. Presciutti, M. Filipponi, A. Nicolini, F. Rossi, Optic-energy performance improvement of exterior paints for buildings, Energy Build. 139 (2017) 690–701, https://doi.org/10.1016/j.enbuild.2017.01.060.
[34] B. Castellani, E. Morini, E. Anderini, M. Filipponi, F. Rossi, Development and characterization of retro-reflective colored tiles for advanced building skins, Energy Build. 154 (2017) 513–522, https://doi.org/10.1016/j.enbuild.2017.08.078.
[35] L.O. Grobe, Characterization and data-driven modeling of a retro-reflective coating in RADIANCE, Energy Build. 162 (2018) 121–133, https://doi.org/10.1016/j.enbuild.2017.12.029.
[36] R. Djedjig, E. Bozonnet, R. Belarbi, Experimental study of the urban microclimate mitigation potential of green roofs and green walls in street canyons, Int. J. Low Carbon Technol. 10 (2013) 34–44, https://doi.org/10.1093/ijlct/ctt019.
[37] A. Sinha, P.A. Horvath, T. Beason, K.R. Roos, Simulation of a financial market: the possibility of catastrophic disequilibrium, Chaos, Solit. Fractals 125 (2019) 13–16, https://doi.org/10.1016/J.CHAOS.2019.05.011.
[38] Z. Li, E. Gariboldi, Reliable estimation of effective thermal properties of a 2-phase material by its optimized modelling in view of Lattice Monte-Carlo simulation, Comput. Mater. Sci. 169 (2019) 109125, https://doi.org/10.1016/J.COMMATSCI.2019.109125.
[39] H. Kanso, R. Patte, D. Ledue, Antiferromagnetic thickness and temperature dependence of the exchange bias properties of Co/IrMn nanodots and continuous films: a Monte Carlo study, J. Magn. Magn. Mater. 491 (2019) 165543, https://doi.org/10.1016/J.JMMM.2019.165543.
[40] V. Ivashko, O. Angelsky, P. Maksimyak, Monte Carlo modeling of ferromagnetism of nano-graphene monolayer within Ising model, J. Magn. Magn. Mater. 492 (2019) 165617, https://doi.org/10.1016/J.JMMM.2019.165617.
[41] G. Son, Y. Son, H. Jeon, J.-Y. Kim, S. Lee, A three-dimensional Monte Carlo model for coarsening kinetics of the bi-continuous system via surface diffusion and its application to nanoporous gold, Scr. Mater. 174 (2020) 33–38, https://doi.org/10.1016/J.SCRIPTAMAT.2019.08.021.
[42] J. Boland, J. Huang, B. Ridley, Decomposing global solar radiation into its direct and diffuse components, Renew. Sustain. Energy Rev. 28 (2013) 749–756, https://doi.org/10.1016/J.RSER.2013.08.023.
[43] D.T. Reindl, W.A. Beckman, J.A. Duffie, Diffuse fraction correlations, Sol. Energy 45 (1990) 1–7, https://doi.org/10.1016/0038-092X(90)90060-P.
[44] M. Pesenti, G. Masera, F. Fiorito, Exploration of adaptive origami shading concepts through integrated dynamic simulations, J. Archit. Eng. 24 (2018) 4018022, https://doi.org/10.1061/(ASCE)AE.1943-5568.0000323.
[45] ASHRAE, ASHRAE Guideline 14, 2014.